

Research Article

Propellant Slosh Force and Mass Measurement

Andrew Hunt ¹, Richard Foster-Turner,¹ and Ross Drury²

¹Atout Process Limited, Ardearn, Wilverley Road, New Milton BH25 5TX, UK

²Flow Measurement and Fluid Mechanics Research Centre, Coventry University, Priory Street, Coventry CV1 5FB, UK

Correspondence should be addressed to Andrew Hunt; ahunt@atoutprocess.com

Received 18 October 2017; Revised 27 March 2018; Accepted 26 April 2018; Published 31 May 2018

Academic Editor: Angel Velazquez

Copyright © 2018 Andrew Hunt et al. This is an open access article distributed under the Creative Commons Attribution License, which permits unrestricted use, distribution, and reproduction in any medium, provided the original work is properly cited.

We have used electrical capacitance tomography (ECT) to instrument a demonstration tank containing kerosene and have successfully demonstrated that ECT can, in real time, (i) measure propellant mass to better than 1% of total in a range of gravity fields, (ii) image propellant distribution, and (iii) accurately track propellant centre of mass (CoM). We have shown that the ability to track CoM enables the determination of slosh forces, and we argue that this will result in disruptive changes in a propellant tank design and use in a spacecraft. Ground testing together with real-time slosh force data will allow an improved tank design to minimize and mitigate slosh forces, while at the same time keeping the tank mass to a minimum. Fully instrumented Smart Tanks will be able to provide force vector inputs to a spacecraft inertial navigation system; this in turn will (i) eliminate or reduce navigational errors, (ii) reduce wait time for uncertain slosh settling, since actual slosh forces will be known, and (iii) simplify slosh control hardware, hence reducing overall mass. ECT may be well suited to space borne liquid measurement applications. Measurements are independent of and unaffected by orientation or levels of g . The electronics and sensor arrays can be low in mass, and critically, the technique does not dissipate heat into the propellant, which makes it intrinsically safe and suitable for cryogenic liquids. Because of the limitations of operating in earth-bound gravity, it has not been possible to check the exact numerical accuracy of the slosh force acting on the vessel. We are therefore in the process of undertaking a further project to (i) build a prototype integrated “Smart Tank for Space”, (ii) undertake slosh tests in zero or microgravity, (iii) develop the system for commercial ground testing, and (iv) qualify ECT for use in space.

1. Introduction

This project was undertaken to test the feasibility of an innovative system that can measure propellant mass in any gravity environment and determine the force or torque on a spacecraft, due to sloshing or movement of the propellant.

The measurement of the mass of the propellant in a spacecraft tank under low or zero gravity conditions remains a significant technical goal. Reference [1] reviews the three most popular techniques, book-keeping, PVT, and thermal propellant gauging (PGS) showing that each has advantages and disadvantages—book-keeping cannot determine load in a multitank configuration when tanks are connected, and PVT accuracy decreases when the amount of the propellant in the tank decreases, while PGS has errors proportional to fill level—so that different methods may be needed at different stages of life. This strong unfulfilled technical need is demonstrated by [2] which gives details of 15 different

measurement techniques and seven separate technology development programs.

The most general technique for GEO satellite applications is book-keeping, but the analysis required to achieve sufficient accuracy at the end of life may be significant [3] as the mass and response of the satellite change with time. The need for differing techniques at different stages of life is reinforced in [4] which concludes that the current best accuracy on remaining life with book-keeping is ± 12 months at 15 years but that improved methods will need to be developed to achieve a suggested target of ± 1 month for future satellites.

Advanced mass measurement technologies under development include radio frequency (RF) [5] and ultrasonic (US) [6]. Although RF and US measurements are clearly capable of making accurate measurements, the interaction of the sensor sensitivity distribution in space due to varying 3-D field strengths with the distribution of fluid means that

there are nonunique solutions for the total mass of fluid for any individual measurement: a small amount of fluid may be present at a position of high field strength giving the same reading as a larger mass of fluid at a position of low field strength. This problem also occurs with single-pair capacitance measurements such as reported in [2], a problem that was at the origin of the development of electrical capacitance tomography (ECT) and which is specifically addressed in the current paper.

The need to extract the propellant from a tank under zero gravity conditions has led to the development of an entire science, nomenclature, and typology (see, e.g., [7, 8]) of propellant management devices (PMDs), rather reminiscent of the evolution of species in nature. Any measurement technique capable of showing 3-dimensional mass distribution in space must be capable of working with PMDs and can be used to help with the design and development of them.

Sloshing of a propellant is also a significant engineering issue, particularly for upper stages and an orbital spacecraft when a high mass fraction of the craft is the propellant itself. Sloshing can cause navigational errors, can starve the propulsion system of the propellant or oxidizer, and has been a factor in some mission failures [9]. Modelling of sloshing in tanks can be undertaken through computational fluid dynamics (CFD) [10] or experiments [11]. The flow structures created are complex and not easily measured; optical pictures and videos are beguiling but not always accurate.

Electrical capacitance tomography (ECT) offers some possible solutions to these needs—accurate mass measurement at any gravity condition or fluid distribution and detailed experimental data to compare with CFD. It may also offer real-time measurements to help with the control system development and operation, giving a 3-D real-time input to the system proposed in [11] for example.

2. Electrical Capacitance Tomography (ECT)

ECT was initially developed at UMIST in the late 1980s, largely under the impetus of Professor Maurice Beck. ECT sensors are made by mounting a series of electrodes around the outside of the flow of interest. The value of capacitance between all pairs of electrodes is measured and the resulting matrix of measurements interpreted through the use of a sensitivity map to give an image or tomograph, typically representing a two-dimensional slice through a vessel [12]. These images are collected at high speed, up to 5000 frames of data per second. ECT research systems have been used in a wide range of applications, including the measurement of coal feedstock [13] and gas-liquid flows [14], while comparisons with other techniques have shown that the mass of product present in a pipe or vessel can be accurately measured [15] and that high levels of detail of complex flow structures can be obtained at a very high speed in real time [16].

A typical modern ECT system is shown in Figure 1, together with a “bare” electrode array. In such a classic sensor, designed for measuring pipe flows, there are 8 lines of electrodes distributed around the pipe circumference, with

each line of electrodes contains 5 sections longitudinally. For any single segment of the eight segments, guards 1, 2, and 3 are electrically connected together, while plane 1 and plane 2 are connected separately. This means that there are 24 electrical connections to the sensor: 3 to each of 8 segments. The function of the guards is to ensure that the electric field is uniform longitudinally while two of the rings of electrodes act as separate measurement “planes.” In pipe flows, this allows velocity to be measured through cross-correlation of the signals from the two planes, while for tanks it allows two sections of the tank to be imaged, thus enabling the tracking of the fluid contents in 3 dimensions, even though the electrical field created is two-dimensional.

The measurement protocol is that in turn one of the longitudinal lines of electrodes is driven with a high-frequency square wave while the current arrival is measured at each of the other 7 electrodes in the two planes. Then the next segment is driven, and the current arrival is measured at each of the other 7 electrodes in the two planes. Because the measurement from the first to the second is the same as the measurement from the second to the first and so on, this leads to 28 independent pairs of measurements in each plane. The capacitance measurement is made using custom electronics, and the image processing is undertaken on a laptop PC. The sensor is connected to the measurement unit by coaxial leads: the advantage of this arrangement is that different sensor heads may be used with the same electronics, and software improvements are easily incorporated. Communication between the PC and the capacitance measurement unit is via high-speed Ethernet, and thus, communications are possible with a control system, but the system is typically used as a stand-alone research device.

The concentration (and hence the mass of the propellant) profile within the vessel is derived from the permittivity distribution inside the ECT sensor, which is calculated from the inter-electrode capacitance measurements. As mentioned above, an 8-segment array yields 28 independent capacitance pairs for each measurement plane—pairs (1,1,2), (1,1,3), (1,1,4), (1,1,5), (1,1,6), (1,1,7), (1,1,8), (1,2,1),..., (1,7,8) for plane 1 and (2,1,2), (2,1,3),..., (2,7,8) for plane 2, where the electrode pairs are plane, driven segment, and receiving segment.

The measured capacitances are small, ranging from less than 10 fF (1 fF being 1 femtofarad or 10^{-15} farad) to a few hundred fF. To put this in perspective, the capacitance in the leads is around 2 pF—200x more than the measurement. The ECT electronics is designed to be immune to capacitance to earth, enabling this level of resolution to be accurately achieved.

In order to reconstruct a numerical image of the fluid distribution within the sensor, it is necessary to solve an inverse problem: given the measured capacitances, what is the permittivity distribution within the sensor? With a 32×32 image matrix and a circular sensor, there are 812 active pixels within the sensor.

The forward problem calculates the capacitances between the electrode pairs from the permittivity distribution inside the sensor where the electric potential at the

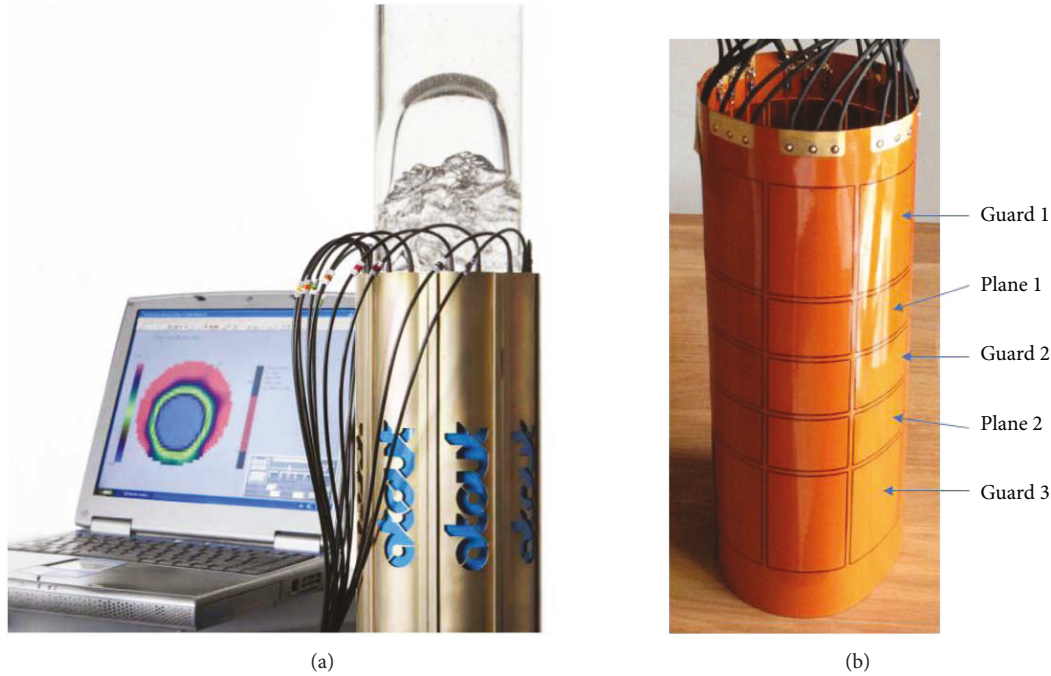


FIGURE 1: (a) A modern ECT system showing an image and sensor and (b) a typical electrode array.

outside of the circle is defined by the potentials applied to the electrodes.

$$\mathbf{C} = \mathbf{S} \cdot \mathbf{K}, \tag{1}$$

where \mathbf{C} is a matrix containing the set of m unique interelectrode pair capacitances (m is 28 for one plane of an 8-electrode sensor as described above), \mathbf{K} is a matrix containing the set of n pixel permittivity values inside the sensor (the permittivity image), and bold characters represent matrices. The sensitivity coefficients \mathbf{S} reflect the coupling between the two electrodes at each pixel location, and these can be calculated by modelling the electric fields which would occur if each electrode acted as a source electrode individually and then integrating the product of the two electric fields over the area of each pixel for each of these pairs. This problem has been addressed by hundreds of papers over the last 20 years or more; for example, [17] first proposed a model for a sensor containing a uniform permittivity and then proved it with a 2-D finite element simulation while [18] showed that this can also be done for a field containing an inclusion of different permittivity.

The inverse problem is represented by

$$\mathbf{K} = \mathbf{S}^{-1} \cdot \mathbf{C}. \tag{2}$$

Equation (2) is of course underdetermined; we are producing 812 pixel values in 2 planes from 28 measurements in each plane, so the inverse of \mathbf{S} , which is not a square, cannot be directly calculated. This inversion is also well-studied, and [19] reviews more than 5 different techniques from more than 40 references concluding that different techniques offer opportunities to trade off accuracy for speed and to obtain the minimum image error. A previous work on imaging fluid flows, reported in [12–16], has

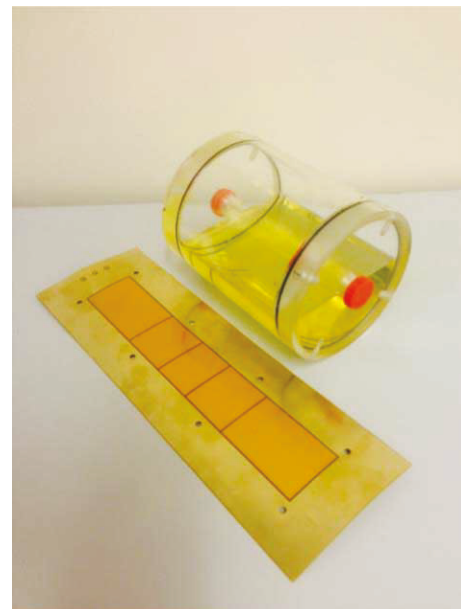


FIGURE 2: Propellant tank used in the experiments with sample electrode.

shown that the simplest of these techniques—linear back projection (LBP)—offers fast reconstruction, and while the images may be less precise than some of the other techniques, the calculation of flow parameter concentration, velocity, and flowrate is accurate and fast. The LPB technique used in the work reported here is an “industry standard” reported in [20] using a numerical calculation of the electric field from each driven electrode and integrating the sensitivity coefficients as described above.

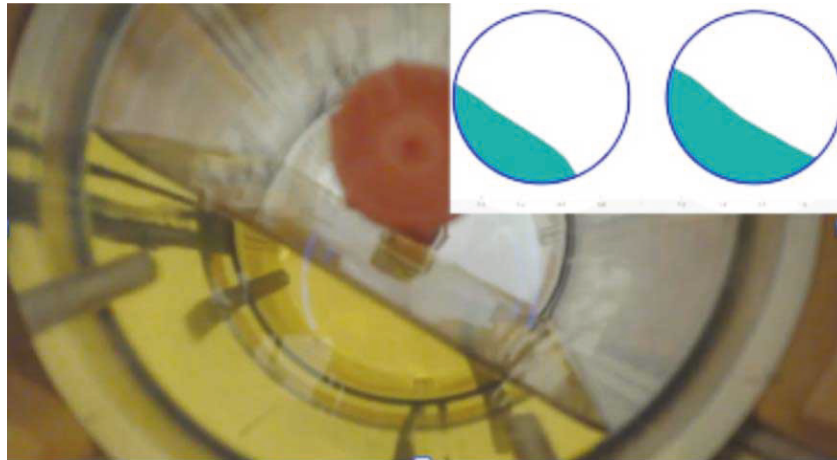


FIGURE 3: Video still from the roll and pitch manoeuvre showing optical (main) and ECT images. Optical video in the main picture and front and rear ECT images in embedded pictures. The ECT images are thresholded so that white is above 50% air, while green is above 50% propellant.

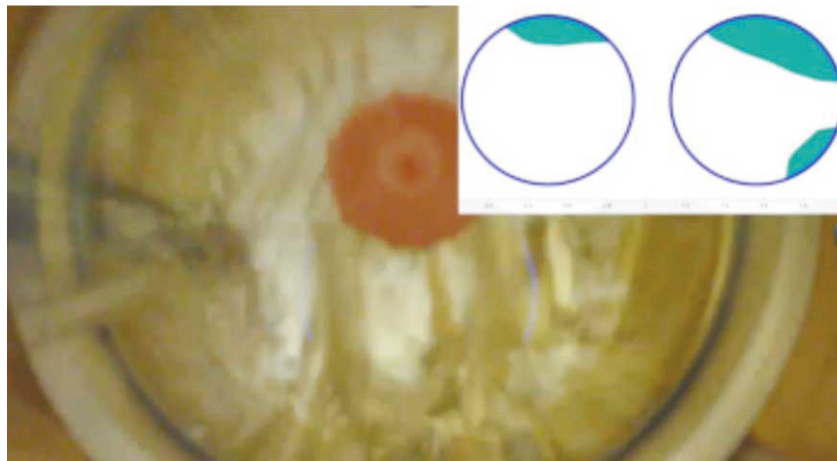


FIGURE 4: Video still from the zero-G shake manoeuvre. Optical video in the main picture and front and rear ECT images in embedded pictures.

3. Test Tank

A simple model propellant tank was constructed from a short section of a transparent acrylic pipe with sealed ends and threaded fill holes, as shown in Figure 2.

The sensor used was a standard Atout APL-S-SL-110 ECT sensor similar to that shown in Figure 1. The sensor body is in eight segments, each of which contains a flexible printed electrode array, one of the printed arrays being shown in Figure 2. The tank was sized exactly to match the length of the central 3 electrodes (plane 1-guard 2-plane 2 in Figure 1), giving a fully guarded plane measurement covering exactly each 1/3 end of the tank. This is not the optimum arrangement for a commercial set of electrodes for propellant tanks but a pragmatic way of establishing the accuracy of measurement and proof of concept within a reasonable timeframe and cost.

The tank was part-filled with kerosene as a test propellant. A video camera was mounted at the end of the sensor

enabling a direct comparison to be made between images from ECT and optical video pictures of the inside of the tank.

The test program consisted of the following protocol:

- (1) Partly fill the sensor to 50% full.
- (2) End-to-end rotation. Starting with sensor vertical, turn horizontal then vertical upside-down, followed by a reverse process to the original orientation.
- (3) Roll, pitch, and shake. Perform roll and pitch manoeuvre followed by three “zero-G” shakes.

4. Experimental Data and Analysis

Twin-plane images were acquired using Atout Sensor Toolkit software and a TFL-5000 capacitance measurement unit. Images were created using Atout Aspin2 data analysis software in a 32×32 voxel grid, each voxel being a cylinder about

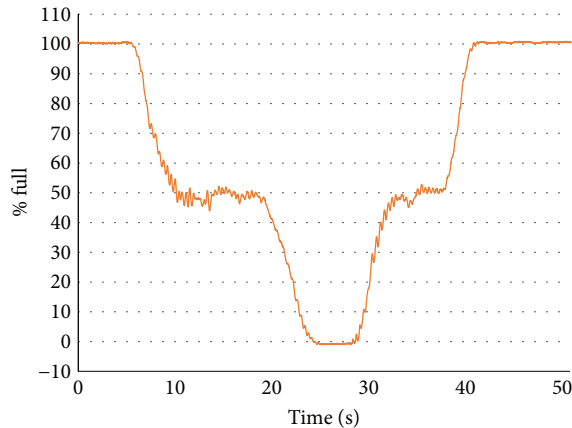


FIGURE 5: Mass (as % full) from ECT measurements in one-half of the tank.

3 × 3 mm square by 30 mm long. Example images are shown in Figures 3 and 4.

Further analysis was performed using specially developed Matlab software routines to display real-time images and real-time calculation of the location of the centre of gravity of the propellant at any moment. Note that the optical video was at a rate of 60 frames per second (fps), while the ECT was acquiring data at 1425 fps. It should also be emphasised that while the optical video is simply a picture, the ECT frame gives a measure of fluid density at every point in space and time.

Using the calculated density and position of each fluid element, the integrated mass in each half of the tank can be calculated.

It can be seen in Figure 5 that when the tank is vertical at the start, the bottom half of the tank is full of the propellant, while the top half is empty (Figure 6). After about 6 seconds, the tank is turned horizontal so that each half is about 50% full: waves can be identified on the graph in both cases. At around 21 seconds, the tank is inverted such that the first half is now empty while the second half is full and so on till the end of the test.

Figure 7 shows the total of the two tank halves on the same time frame. It can be seen that the error is less than ±2% for the whole test with an rms error of better than 1%. Even the waves and ripples are completely averaged out.

ECT images give a calibrated cross-section of mass distribution within the instrumented vessel. This distribution is measured in two halves, allowing the centre of mass (CoM) to be determined in each half, and thus within the whole vessel. X-Y position and movement are determined within each half, while the Z-Y forces are calculated from the moments of the two halves combined.

5. A Simplified Fluid Dynamic Model to Determine Slosh Force

The case considered here is that of a closed vessel containing a quantity of fluid that is varying slowly with time as the propellant is used. The slosh forces occur on a timescale of

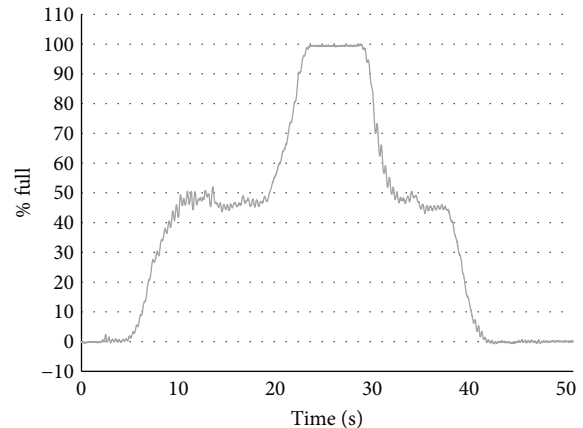


FIGURE 6: Mass (as % full) in the second half of the tank.

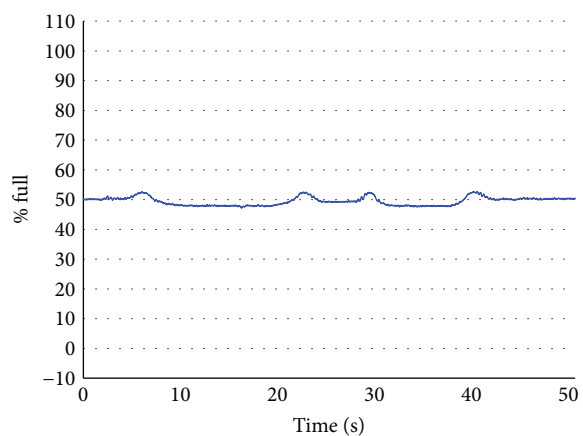


FIGURE 7: The average of the two tank half values from the end-to-end rotation.

fractions of a second during flight events, such as accelerations or turbulence, while the propellant is used up over a period of months or years. Given this difference in timescale, we will consider here that for the purposes of determining slosh forces, the fluid mass in the tank can be considered constant for the fraction of a second that the slosh force is calculated.

The calculation of the movement of fluid in a sloshing tank is a complex fluid mechanical problem [21], but the primary complexity is calculating the movement of the fluid. The huge advantage of real-time ECT measurement is that the fluid movement does not have to be modeled: it is directly measured. The data shown here is taken at a rate of 1425 complete frames of data per second. Image display is rather slower, no more than 20 fps being necessary to depict smooth movement to the human eye. The recorded data can be retained at any required frequency.

The movement of fluid leads to dynamic forces on the vessel, and this movement can be represented by the sum of the motion of any number of fluid elements.

Figure 8 shows a nominal fluid element that is within the tank. While there is no contact between the fluid and the tank

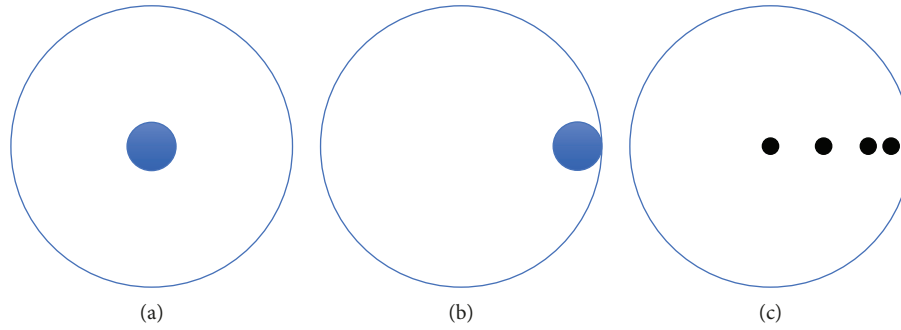


FIGURE 8: Schematic diagram of fluid element motion under zero gravity with the tank moving left. Fluid element in motion relative to the tank (a), fluid element in contact with the tank wall prior to distortion (b), and movement of the centre of mass at equal time steps (c).

wall, the element is free to move with the acceleration forces (gravity or other acceleration) without exerting any force on the tank. As the fluid comes into contact with the tank wall, there is a force from the tank onto the element and the equal and opposite reaction force is the slosh force. The element will distort as a result of the force, and the movement of the CoM of the element (shown to the right of the figure) will slow down. The exact distortion or future movement of the fluid element will depend on many other factors, but the net slosh force can always be determined from the rate of change of the velocity of the element CoM. This argument can be applied to all fluid particles of any size, and the total slosh force can be calculated from the sum of all the motions of all the elemental CoMs, which is equivalent to the motion of the overall CoM of fluid within the tank.

Once the fluid has stabilised, it will occupy the position of minimum energy within the tank, as shown in Figure 9. The location of the fluid will change to align with the resultant acceleration vector, and while there will be a force of the fluid on the tank (mass \times acceleration), the CoM is stationary in the frame of reference of the tank.

Thus, the slosh force, defined as the dynamic force on the tank induced by fluid motion, is additional to the normal “weight” of the fluid and can be determined from the rate of change of the CoM of the propellant within the tank. In contrast, the position of the CoM is independent of the absolute “gravity” force once the fluid is stable in a stable acceleration environment. ECT thus measures directly the slosh force of interest, without contribution from the pseudo-static “body” force.

6. Experimental Slosh Test

The experimental tests were undertaken using the same tank as in previous work reported in [16] (see Figure 2), but the electrodes were modified to image the entire tank contents in two halves mounted in a sensor similar to that shown earlier.

A simple test case is shown here to examine the accuracy of the resolution of the measurement of CoM. The sensor, tank, and electronics were mounted freely in a cylindrical cage, which could be rotated and shaken. The test results shown in Figure 10 consist of rotation and dwell at 90 degrees (110 to 160 sec), rotation and dwell at 180 degrees (160 to 190 sec), rotation and dwell at 270 degrees (190 to

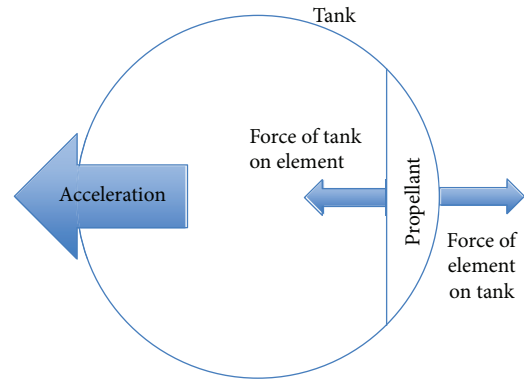


FIGURE 9: Minimum energy fluid distribution with steady acceleration vector.

230 sec), and rotation and dwell at 360 degrees (230 to 250 sec) followed by a rapid rotation through 360 degrees (250 to 260 sec) and a series of 3 longitudinal shakes (300 to 330 sec).

Figure 11 shows an expanded scale of the same test, part of the first shake event. The sloshing of fluid from end to end of the tank can be clearly seen by the masses shown in the two halves being cyclic and out of phase with a magnitude of $\pm 12\%$ or so, while the total indicated mass from the ECT system shows well under $\pm 0.5\%$ variability.

Accurate tracking of the CoM is the proof of the accuracy of the slosh force measurement by ECT. The ECT estimate of fuel mass is 21% of the tank’s full mass, corresponding to a CoM of $0.347d$ where d is the tank’s internal diameter. Thus, during the rotation events, the CoM should describe an exact circle of radius 0.347 on an end view of the tank. Such a view is shown in Figure 12, and the precision of the locus is clear. The smoother blue circle is the slow rotate and dwell part of the experiment, while the more variable path is the rapid rotation.

For the shake events, the CoM may move anywhere within the tank but is restrained by the outer envelope which is the CoM for the minimum energy position at each angle, a shape resembling a pendulum, marking the outer boundary of the locus in Figure 13. In all cases, it is clear that the CoM is accurately tracked through all predictable positions. Note also that at the 90-degree “dwell” points, there are

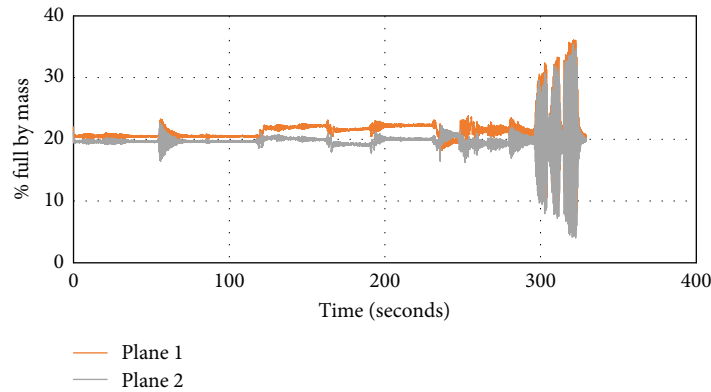


FIGURE 10: Total mass (0.2 = 20% full) in the two tank halves. Sloshing between the two halves, plane 1 and plane 2 are shown clearly.

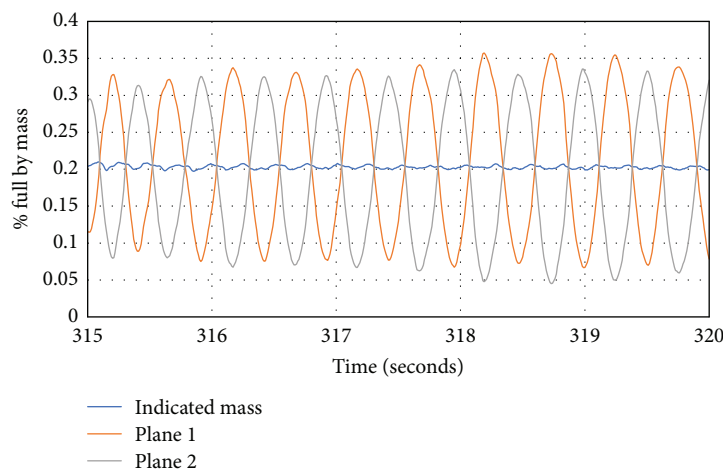


FIGURE 11: Expanded section of the previous graph.

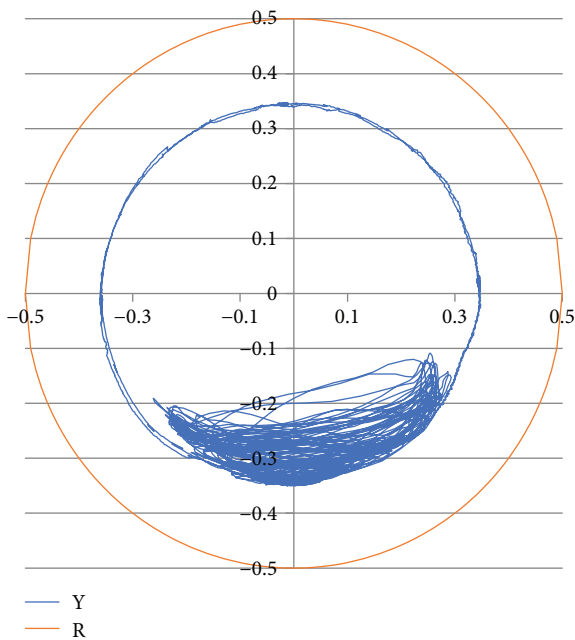


FIGURE 12: Locus of the centre of mass (CoM) in the X-Y plane for tank 20% full (blue line) with tank internal envelope (orange line).

several thousand repeat points that show less variation than the thickness of the plot line.

7. Conclusions

We have successfully demonstrated that ECT can be used to

- (i) measure propellant mass to better than 1% of the total in a wide range of gravity fields over several fill levels
- (ii) image propellant distribution in real-time
- (iii) accurately track propellant CoM.

Because of the limitations of operating in earth-bound gravity, it has not been possible to check the exact numerical accuracy of the slosh force acting on the vessel. We therefore plan the following next steps:

- (i) Build a prototype integrated “Smart Tank for Space”
- (ii) Undertake slosh tests in zero or microgravity, with accurate force measurements on a suspended vessel compared with ECT measurements

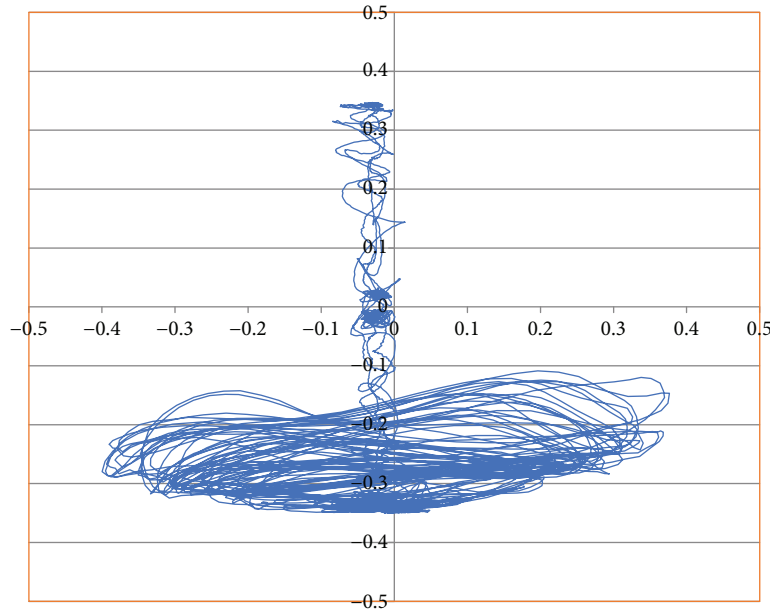


FIGURE 13: Locus of the CoM in the Z-Y plane (blue line) compared with tank internal envelope (orange line).

- (iii) Use the system for commercial ground testing
- (iv) Develop a qualification program for the use of ECT in space.

Conflicts of Interest

The authors declare that there is no conflict of interest regarding the publication of this paper.

Acknowledgments

The authors would like to acknowledge the financial support of UK Space Agency, Atout Process Limited, and Coventry University in funding this work.

References

- [1] B. Yendler, "Review of propellant gauging methods," *44th AIAA aerospace sciences meeting and exhibit*, 2006, Reno, Nevada, January 2006, 2006.
- [2] F. T. Dodge, "Propellant mass gauging: database of vehicle applications and research and development studies," US Patent NASA/C-2008-215281, 2008.
- [3] C. Burghardt, F. Meissner, H. Enke, S. Oehler, and J. Letschnik, "Propellant endurance prognosis for GEO operations," in *American Institute of Aeronautics and Astronautics Conference Paper*, Stockholm, June 2012.
- [4] R. C. van Benthem, J. van Es, P. van Put, and R. Matthijsen, "Accuracy analysis of propellant gauging systems," *43rd International Conference on Environmental Systems (ICES)*, 2013, Vail, CO, USA, July 2013, 2013.
- [5] G. A. Zimmerli, K. R. Vaden, M. D. Herlacher, D. A. Buchanan, and N. T. Van Dresar, "Radio frequency mass gauging of propellants," US Patent NASA/TM-2007-214907, 2007.
- [6] F. Murolo, C. Bihl, P. Pili, M. Klinc, and R. Brandt, "The ultrasonic gauging sensors: results of an innovative spacecraft propellant measurement method," in *SpaceOps 2014 Conference*, Pasadena, CA, USA, May 2014.
- [7] W. Tam, P. Behruzi, D. Jaekle, and G. Netter, "The evolutionary forces and the design and development of propellant management devices for space flight in Europe and the United States," in *Space Propulsion Conference 2016-SP2016_3124615*, Rome, Italy, May 2016.
- [8] J. W. Hartwig, "Propellant management devices for low-gravity fluid management: past, present, and future applications," *Journal of Spacecraft and Rockets*, vol. 54, no. 4, pp. 808–824, 2017.
- [9] N. Fries, P. Behruzi, T. Arndt, M. Winter, G. Netter, and U. Renner, "Modelling of fluid motion in spacecraft propellant tanks – sloshing," *Space Propulsion 2012 Conference*, 2012, Bordeaux, May 2012, 2012.
- [10] H. Q. Yang and J. Peugeot, "Propellant sloshing parameter extraction from CFD analysis," *46th AIAA/ASME/SAE/ASEE Joint Propulsion Conference & Exhibit*, 2010, Nashville, TN, USA, July 2010, 2010.
- [11] H. Jetzschmann and S. B. Strauch, "Model based active slosh damping experiment," *GNC2017: 10th International ESA Conference on Guidance, Navigation and Control Systems*, 2017, Salzburg, Austria, May-June 2017, 2017.
- [12] A. Hunt, J. Pendleton, and Y. Ladam, "Visualisation of two-phase gas-liquid pipe flows using electrical capacitance tomography," in *ASME 7th Biennial Conference on Engineering Systems Design and Analysis*, Manchester UK, July 2004.
- [13] B. J. Azzopardi, K. Jackson, J. P. Robinson, R. Kaji, M. Byars, and A. Hunt, "Fluctuations in dense phase pneumatic conveying of pulverised coal measured using electrical capacitance tomography," *Chemical Engineering Science*, vol. 63, no. 9, pp. 2548–2558, 2008.
- [14] B. J. Azzopardi, L. A. Abdulkareem, D. Zhao et al., "Comparison between electrical capacitance tomography and wire mesh

- sensor output for air/silicone oil flow in a vertical pipe,” *Industrial & Engineering Chemistry Research*, vol. 49, no. 18, pp. 8805–8811, 2010.
- [15] A. Hunt, “Weighing without touching: applying electrical capacitance tomography to mass flowrate measurement in multiphase flows,” *Measurement and Control*, vol. 47, no. 1, pp. 19–25, 2014.
- [16] A. Hunt and R. Foster-Turner, “Real time multi-phase mass and density measurement of propellant in zero G,” in *UK Space Propulsion Workshop, 29 October 2015*, Imperial War Museum, London UK, 2015.
- [17] J. P. Oakley and M. S. Bair, “A mathematical model for the multi-electrode capacitance sensor [and tomographic reconstruction algorithm],” *Measurement Science and Technology*, vol. 6, no. 11, pp. 1617–1630, 1995.
- [18] K. L. Ostrowski, S. P. Luke, and R. A. Williams, “Application of conjugate harmonics to electrical process tomography,” *Measurement Science and Technology*, vol. 7, no. 3, pp. 316–324, 1996.
- [19] W. Q. Yang and L. Peng, “Image reconstruction algorithms for electrical capacitance tomography,” *Measurement Science and Technology*, vol. 14, no. 1, pp. R1–R13, 2003.
- [20] P. T. L. Application Note AN7, “Calculation of circular ECT sensitivity maps and inter-electrode capacitance pair values,” *Process Tomography Limited, UK*, 2000, <http://www.tomography.com>.
- [21] G. Yan and S. Rakheja, “Fluid structure interaction induced by liquid slosh in partly filled road tankers,” *World Academy of Science, Engineering and Technology International Journal of Mechanical, Aerospace, Industrial, Mechatronic and Manufacturing Engineering*, vol. 4, no. 10, 2010.



Hindawi

Submit your manuscripts at
www.hindawi.com

